Dalton Transactions

An international journal of inorganic chemistry

Accepted Manuscript

ROYAL SOCIETY OF CHEMISTRY

rsc.li/dalton

View Article Online
DOI: 10.1039/C9DT03322J

Journal Name

ARTICLE

Neutral nano-polygons with ultrashort Be-Be distances

Wen-Yan Tong,[a,‡] Tao-Tao Zhao,[a,‡] Xue-Feng Zhao,[a] Xiaotai Wang,[a,b] Yan-Bo Wu*[a] and Caixia Yuan*[a]

Received 00th January 20xx,
Accepted 00th January 20xx

DOI: 10.1039/x0xx00000x

www.rsc.org/

The ultrashort metal-metal distances (USMMDs, $d_{M\text{-}M}$ < 1.900 Å) had been realized computationally between main group metal beryllium. However, due to their ionic charge state or the insufficient stability on electronic structures and/or thermodynamic stabilities, the known species with ultrashort Be-Be distances are unsuitable for synthesis in the condensed phase, which deters applications of such interesting structures from being explored. In the present work, using our previously reported global minima species $[XH_3\text{-}Be_2H_3\text{-}XH_3]^+$ (X = N, P) with the ultrashort Be-Be distances and well-defined electronic structures as the parent molecules, we had designed a series of neutral polygons retaining ultrashort Be-Be distances. These polygons also possess the well-defined electronic structures and good thermodynamic stabilities, which can be demonstrated by the large HOMO-LUMO gaps of 6.20–7.68 eV, the very high vertical detachment energies (VDEs) of 8.96–11.29 eV, the rather low vertical electron affinities (VEAs) of –1.21 to +1.78 eV, and the unexpectedly high formation energies relative to the building blocks of E^- and $Be_2H_3^+$ (–105.2 to –153.2 kcal/mol for the formation of a E-Be bond). The good stability with regard to electronic structures and thermochemistry revealed their high feasibility to be synthesized in the condensed phase. We invite the experimental studies on these intersting nano-polygons to realize structures with USMMDs between main group metals and explore the possible application.

Introduction

An exciting goal in metal-metal bonding chemistry is to achieve the species with ultrashort metal-metal distances (USMMDs).[1] Here, the prefix "ultra" is used to stress the feature of "short" and the rareness. Originally, the USMMDs were realized through forming the homonuclear high-order bonds between first row transition metals, like Cr,[2] which had found useful application in synthetic chemistry.[3]

However, achieving the USMMDs between main group metals cannot be realized by forming homonuclear high-order bonds due to the limitation of electronic shell structures: The alkali and alkaline earth metals do not have enough valence electrons to support the homonuclear triple bonds and the p-block metals are heavy and suffer from the inert pair effect,[4] which deters the formation of triple bonds.

Nevertheless, the USMMDs have been realized between beryllium atoms with the aid of auxiliary bridging atoms.[5] The ultrashort Be-Be distances can be realized covalently through the formation of three bonding orbitals between two Be atoms,[5b,5g] electrostatically through the strong Coulomb interactions among the positively charged Be atoms and the negatively charged bridging atoms, [5b-5e] or the combination of both covalent and electrostatic effects.[5f] However, no species with ultrashort Be-Be distances had been achieved synthetically (in the condensed phase), which makes it hard to explore the application of such novel structures, so the synthetically viable species should be a target of computational design in this field. Here, though the charged ions can be synthesized as well, they are more preferred by the gas phase generation due to the facility of separation in the magnetic field. Therefore, the neutral molecules with good electronic structures and thermodynamic stabilities are highly desired.

In known species with ultrashort Be-Be distances, the $[R\text{-}Be_2H_3\text{-}R']^q$ (R and R' are electron donors, q = 0, 1) molecules are unique for their well-defined electronic structures, as reflected by the large HOMO-LUMO gaps up to 8.51 eV at the B3LYP level.[5g,6] In general, the Be_2H_3 core moiety can be seen as a mono-cationic Lewis acid, which is stabilized by terminal Lewis bases R and R'. Note that if R = R', it will always get the ionic species. So, the simplest way to neutralize such structure would be the employment of a neutral and an anionic terminal groups. Previously, Li *et al*. had reported the such type of neutral species $Ng\text{-}Be_2H_3\text{-}R$ (Ng is a noble gas and R can be H, CH_3, and F).[6] However, according to our extensive exploration on their potential energy surfaces, none of them are thermodynamically stable.[7] In contrast, some cationic species $X\text{-}Be_2H_3\text{-}X^+$ (X = NH_3, PH_3, or noble gases) with same ligand at both terminals of Be_2H_3 core could be stable thermodynamically. Such results suggest that symmetric species may possess the good thermodynamic stability. Therefore, alternate to use a neutral and an anionic mono-dentate ligands, another possible way to neutralize the molecules would be the employment of mono- anionic

[a] The Key Laboratory of Energy Conversion and Storage of Shanxi Province, Institute of Molecular Science, Shanxi University, Taiyuan 030006, Shanxi, People's Republic of China. *Email address: wyb@sxu.edu.cn, cxyuan@sxu.edu.cn.
[b] Department of Chemistry, University of Colorado Denver, Campus Box 194, P.O. Box 173364, Denver, Colorado 80217-3364, United States.

†Electronic Supplementary Information (ESI) available: The AdNDP results for representative polygons, the table summarizing the NBO results, the full form of ref. 12 and 13, the optimized structures of some polygons, and the Cartesian coordinates of all species reported in this work. See DOI: 10.1039/x0xx00000x

‡These authors contribute equally to this work.

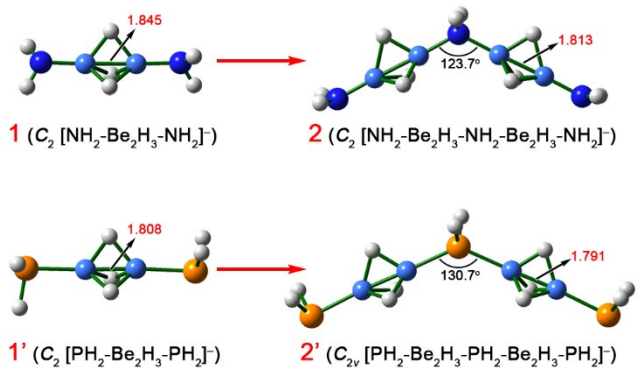

Fig. 1. B3LYP/def2-TZVPP-optimized structures of linear molecules **1**, **2**, **1'**, and **2'**. The Be-Be distances (in Å), other interatomic distances (in Å), and natural charges (in |e|) are shown in red, black, and italic blue fonts, respectively.

bidentate ligands. Geometrically, if two lone pairs locate on different atoms, it would be relatively hard to find the proper symmetric ligand. Consequently, our attention was paid to the mono-anionic ligand with at least two lone pairs on one atom. In this work, starting from NH_2^- and PH_2^-, we systematically examined the feasibility of a series of mono-anions for designing the neutral cyclized structures and found that corresponding species retained both USMMDs and good electronic structures.

Results and Discussion

1. Design of $(XH_2\text{-}Be_2H_3)_n$ (X = N, P; *n* = 3–8)

Employing our previously reported XH_3-Be_2H_3-XH_3^+ (X = N, P) species as the parent molecules, we first replaced the XH_3 terminal group with the isoelectronic species XH_2^- (X = N, P), leading to the fragmental mono-anionic compounds NH_2-Be_2H_3-NH_2^- (**1**) and PH_2-Be_2H_3-PH_2^- (**1'**) (see Fig. 1). **1** and **1'** are the energy minima with C_2 symmetry at the B3LYP/def2-TZVPP. The HOMO-LUMO gaps for **1** and **1'** are 4.91 and 5.71 eV, respectively (Table 1), which are the suggestions of their relatively good electronic structures. Though mono-anions **1** and **1'** suffer from the so-called "Coulomb explosion effect", the Be-Be distances are 1.845 and 1.808 Å in **1** and **1'**, respectively, being shorter than 1.900 Å and thus being the eligible USMMDs.

Since NH_2^- and PH_2^- both have two lone pairs, it is practicable for each of them to form two dative bonds with $Be_2H_3^+$. Consequently, the structures of **1** and **1'** can be extended by adding a NH_2-Be_2H_3 or PH_2-Be_2H_3 moiety, resulting in the mono-anionic species NH_2-Be_2H_3-NH_2-Be_2H_3-NH_2^- (**2**) and PH_2-Be_2H_3-PH_2-Be_2H_3-PH_2^- (**2'**), respectively. At the B3LYP/def2-TZVPP, **2** and **2'** are the energy minima adopting C_2 and C_{2v} symmetries, respectively. The HOMO-LUMO gaps of **2** and **2'** are 4.97 and 5.45 eV, respectively, similar to those for **1** and **1'**. Since **2** and **2'** are larger than **1** and **1'**, but are still mono-anionic, the weakened Coulomb explosion effect leads to the shortened Be-Be distances of 1.813 and 1.791 Å in **2** and **2'**, respectively.

Given that adding NH_2-Be_2H_3 or PH_2-Be_2H_3 to **1** and **1'**, respectively, does not change their charge state, it is easy to think of the cyclized structures with equal number of XH_2^- and $Be_2H_3^+$ building blocks, which are the desired neutral polygons possibly with the USMMDs. In this work, the designed polygons are named as ***n*-E**, where ***n*** denotes the number of the Be_2H_3

Table 1. The point groups (PG), lowest vibrational frequencies (ν_{min}, in cm^{-1}), HOMO-LUMO gaps (Gap, in eV), and the formation energies for each X-Be bond ($FE_{X\text{-}Be}$) (X = N, P, O, S, F, Cl, Br) at the B3LYP/def2-TZVPP level for structures designed in this work. Corresponding VDEs and VEAs (in eV) are calculated at the OVGF/def2-TZVPP level.

	PG	ν_{min}	Gap	VDE	VEA	$FE_{X\text{-}Be}$
1	C_2	138	4.91	4.08	4.93	
2	C_2	14	4.97	5.04	4.24	
3-NH_2	D_{3h}	154	6.28	9.44	1.05	−149.3
4-NH_2	D_{4h}	47	6.53	9.67	1.12	−152.6
5-NH_2	D_{5h}	23	6.83	9.93	1.21	−153.2
6-NH_2	D_{6h}	9	6.88	9.99	1.19	−153.2
7-NH_2	C_2	9	6.90			−153.2
8-NH_2	D_{2d}	8	6.91			−153.2
1'	C_2	83	5.71	4.55	4.91	
2'	C_{2v}	24	5.45	5.48	3.75	
3-PH_2	D_{3h}	88	7.10	10.27	1.21	−119.4
4-PH_2	D_{4h}	26	6.99	10.28	1.21	−121.2
5-PH_2	D_{5h}	17	7.10	10.31	1.10	−121.6
6-PH_2	D_{6h}	10	7.00	10.23	1.05	−121.7
7-PH_2	D_{7h}	4	7.05			−121.7
8-PH_2	D_{2d}	3	7.03			−121.8
3-OH	C_s	130	6.20	9.77	0.87	−146.4
4-OH	C_{2v}	47	6.38	9.91	0.93	−150.7
5-OH	C_2	10	6.56	10.12	1.03	−152.0
6-OH	D_{3d}	12	6.52	10.09	1.05	−152.3
3-SH	C_s	105	7.01	10.26	1.00	−118.0
4-SH	C_{4v}	21	7.17	10.46	1.03	−119.6
5-SH	C_s	8	7.26	10.50	0.96	−119.9
6-SH	D_{3d}	9	7.35	10.59	0.90	−119.6
3-F	D_{3h}	153	6.76	10.51	0.86	−137.4
4-F	D_{2d}	53	7.11	10.81	0.96	−141.5
5-F	C_2	17	7.52	11.16	1.06	−142.9
6-F	D_{3d}	13	7.53	11.29	0.94	−143.4
3-Cl	D_{3h}	87	7.32	10.83	1.09	−112.4
4-Cl	D_{2d}	19	7.58	11.03	1.10	−114.4
6-Cl	D_{5h}	7	7.68	11.00	0.96	−114.7
6-Cl	S_6	9	7.64	11.02	0.89	−114.7
3-Br	D_{3h}	69	7.30	10.77	1.07	−105.2
4-Br	D_{2d}	11	7.29	10.67	1.06	−106.8
5-Br	C_2	1	7.39	10.69	0.91	−107.1
6-Br	S_6	7	7.43	10.79	0.87	−106.8
3-$N(CH_3)_2$	D_{3h}	69	6.70	9.26	1.46	−137.5
4-$N(CH_3)_2$	D_{4h}	24	6.98	9.41	1.54	−140.7
5-$N(CH_3)_2$	D_{5h}	16	7.23	9.67	1.54	−141.1
6-$N(CH_3)_2$	D_{6h}	7	7.23	9.68	1.78	−141.0
3-$P(CH_3)_2$	D_{3h}	36	6.56	8.99	1.41	−125.3
4-$P(CH_3)_2$	D_{4h}	13	6.42	8.96	1.48	−127.0
5-$P(CH_3)_2$	D_{5h}	9	6.59	9.04	1.43	−127.4
6-$P(CH_3)_2$	C_{6v}	1	6.49	8.99	1.38	−127.6
3-OCH_3	C_{3v}	59	6.56	9.60	1.41	−135.9
4-OCH_3	C_{2h}	18	6.75	9.57	1.53	−140.5
5-OCH_3	C_{5v}	8	7.06	9.79	1.52	−141.6
6-OCH_3	D_{3d}	12	7.07	9.78	1.44	−141.7
3-SCH_3	C_{3v}	55	6.76	9.76	1.34	−119.8
4-SCH_3	D_{2d}	18	6.92	9.91	1.39	−121.6
5-SCH_3	C_{5v}	6	6.65	9.72	1.29	−121.7
6-SCH_3	D_{3d}	7	7.08	9.92	1.24	−121.6

View Article Online
DOI: 10.1039/C9DT03322J

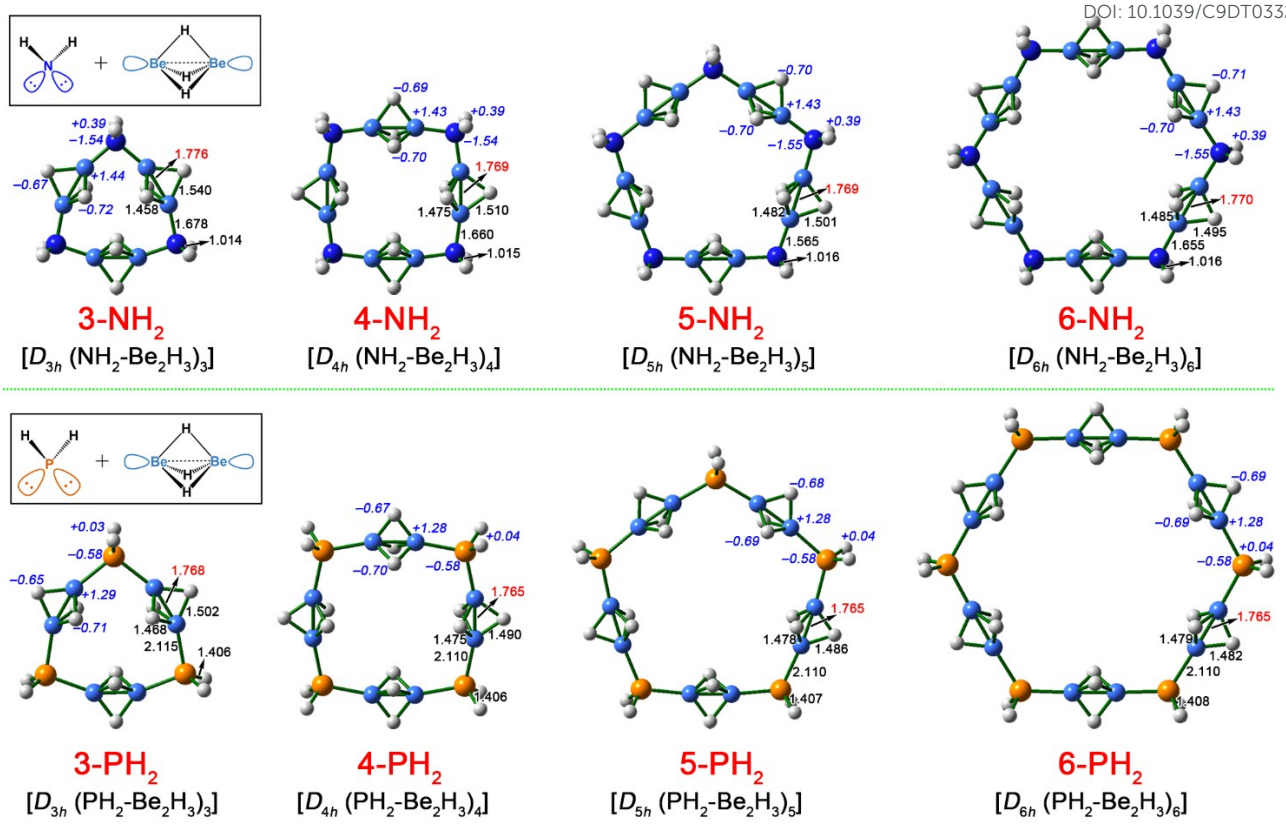

Fig. 2. B3LYP/def2-TZVPP-optimized structures of polygonal molecules **3-NH$_2$** to **6-NH$_2$** and **3-PH$_2$** to **6-PH$_2$**. The Be-Be distances (in Å), other interatomic distances (in Å), and natural charges (in |e|) are shown in red, black, and italic blue fonts, respectively.

edges in the polygons and **E** denotes the mono-anions locating at the vertexes of the polygons. For example, **3-NH$_2$** represents a trigonal structure with three Be_2H_3 edges linked by three NH_2 moieties at the vertexes.

Using NH_2 and PH_2 as the vertexes, we had constructed the representative polygons ***n*-NH$_2$** and ***n*-PH$_2$** (n = 3–6). Their B3LYP/def2-TZVPP-optimized structures are shown in Fig. 2. As the figure shows, the triangles to hexagons adopt the highly symmetric D_{nh} (n = 3–6) structures. Geometrically, the largest intramolecular interatomic distances in ***n*-NH$_2$** and ***n*-PH$_2$** (n = 3–6) range from 6.75 to 13.97 Å in the B3LYP/def2-TZVPP-optimized structures, *i.e.* 0.675–1.397 nm, so it is reasonable to classified these polygonal structures as the nano-molecules. Being the neutral species, ***n*-NH$_2$** and ***n*-PH$_2$** (n = 3–6) do not involve in Coulomb explosion effect. As a result, the Be-Be distances range from 1.769 to 1.776 Å for ***n*-NH$_2$** and from 1.765 to 1.768 Å for ***n*-PH$_2$** (Fig. 2). In comparison with **2** and **2'**, the Be-Be distances are further shortened.

To calibrate the B3LYP functional, the species **1**, **1'**, **2**, **2'**, ***n*-E** (n = 3–5, E = NH_2, PH_2) were selected as the representatives for the re-optimization using both M06-2X-D3[8] functional and *ab initio* method MP2. In M06-2X-D3/def2-TZVPP results, the geometries for **4-NH$_2$** and **4-PH$_2$** were slightly distorted to the lower D_{2d} symmetry, while In MP2/def2-TZVPP results, only the geometry of **4-NH$_2$** has the similar distortion. Nevertheless, the difference between the B3LYP- and M06-2X-D3- or MP2-optimized geometries lies only in the positions of bridging H atoms. Since such H atoms have relatively high rotational freedom (similar to H atoms of methyl group), the B3LYP- and MP2-optimized structures should essentially represent the same species. The MP2/def2-TZVPP-optimized structures for other species all adopt the symmetric D_{nh} structures, which have very similar geometric parameters to those optimized at the B3LYP/def2-TZVPP level. Therefore, B3LYP functional should be accurate enough for current system and the following discussions are based on the B3LYP results.

We then examined the possibility of forming the larger heptagons and octagons at the B3LYP/def2-TZVPP level. As shown in Fig. S1, only heptagonal **7-PH$_2$** adopt the highly symmetric D_{7h} structure, while the heptagonal **7-NH$_2$** is distorted to a lower C_2 structure. For octagons, both **8-NH$_2$** and **8-PH$_2$** adopt the lower D_{2d} rather than highly symmetric D_{8h} structures. Nevertheless, the distortions in geometries is only the results of structural softness, it does not obviously influence the electronic structure, which can be reflected by the large HOMO-LUMO gaps of 6.90/6.91 eV for **7-NH$_2$**/**8-NH$_2$** and those of 7.05/7.03 eV for **7-PH$_2$**/**8-PH$_2$**. Simultaneously, **7-NH$_2$** and **8-NH$_2$** possess the Be-Be distances of 1.767 to 1.771 Å, while **7-PH$_2$** and **8-PH$_2$** both possess the Be-Be distance of 1.765 Å, which are almost identical to those in **3-NH$_2$** to **6-NH$_2$** and **3-PH$_2$** to **6-PH$_2$**, respectively, as well. The studies on heptagons and octagons indicate that the even larger polygons may adopt the asymmetric geometries, but they may inherit the good electronic structures and the ultrashort Be-Be distances from

View Article Online
DOI: 10.1039/C9DT03322J

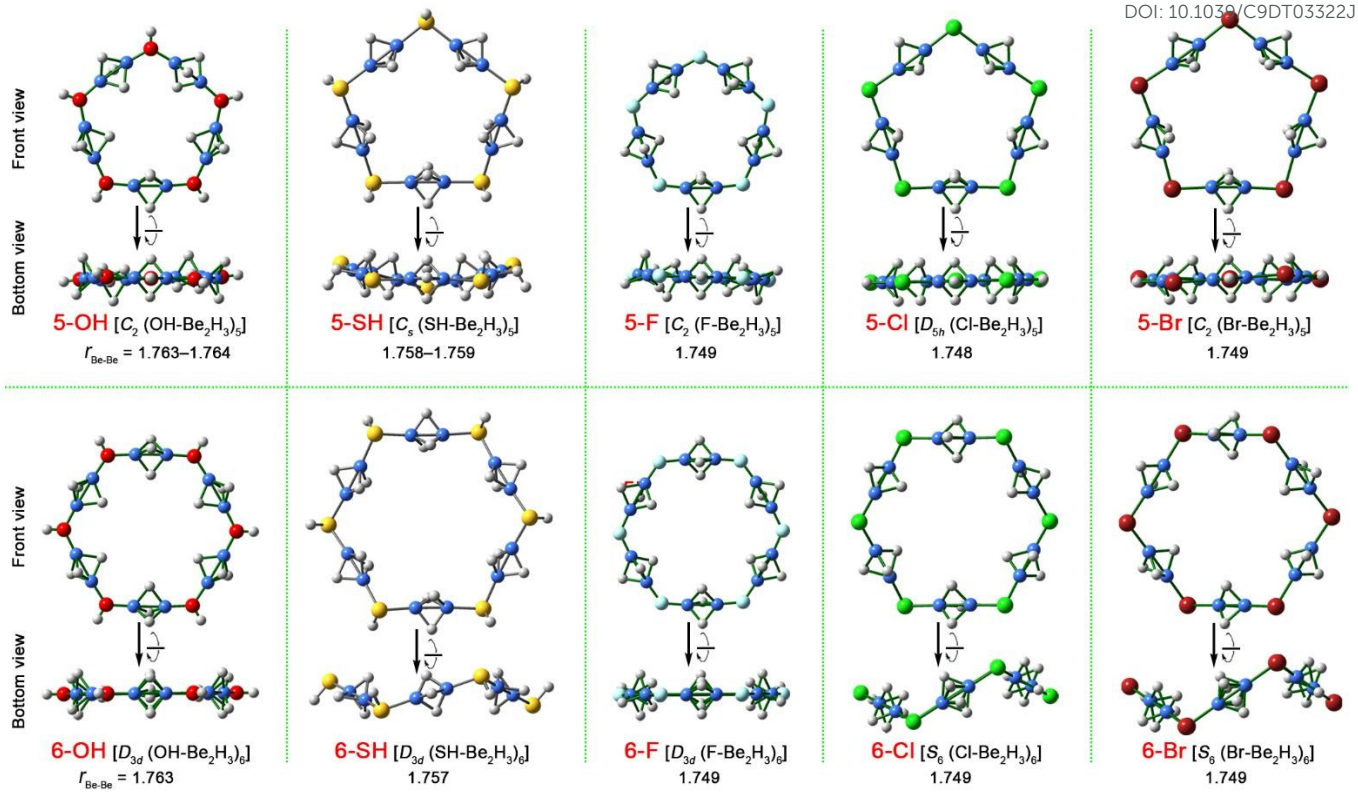

Fig. 3. B3LYP/def2-TZVPP-optimized structures of pentagons and hexagons with OH, SH, F, Cl, and Br moieties as the vertexes.

their smaller analogues. Therefore, for the studies on polygons with other types of vertexes, only triangles to hexagons are discussed.

2. Screening other mono-anions

Encouraged by the effective practice in using NH_2^- and PH_2^- to design the polygonal structures with USMMDs, we further examined the feasibility of a series of mono-anions for the assembly with Be_2H_3 moiety. Fig. 3 shows the optimized structures of pentagons and hexagons of ***n*-E** (n = 5, 6 and E = OH, SH, F, Cl, Br), while corresponding triangles and tetragons are given in the Fig. S2 in †ESI. As the figures show, for trigon and tetragon with OH^- as the vertexes, the H atoms on O derivate clearly from the planar O-Be framework, suggesting that O atoms are in sp^3 hybrid state, while the H atoms on O atoms of corresponding pentagon and hexagon adopt the almost co-planar position to the O-Be framework, indicating the sp^2 hybrid O atoms. We note that the O-Be polygonal frameworks almost keep planar, which pronounces the relatively rigid polygonal structures. As a comparison, the H atoms on S atoms of ***n*-SH** are all out of corresponding Be-S-Be planes, suggesting that all S atoms adopt the sp^3 hybrid state. The S-Be cycles in ***n*-SH** (n = 3–5) are in planar or quasi-planar arrangements, while that in **6-SH** is in zig-zag arrangement. The HOMO-LUMO gaps in ***n*-OH** polygons range from 6.20 to 6.56 eV. Though they are a little narrower than the ***n*-NH_2** and ***n*-PH_2**, such big values are still the sign of good electronic structure. The Be-Be distances in ***n*-OH** polygons range from 1.764 to 1.772 Å and those in ***n*-SH** from 1.757 to 1.762 Å, similar to those in ***n*-NH_2** or ***n*-PH_2** polygons, respectively and being the USMMDs.

For polygons with halogen anions (F^-, Cl^-, Br^-) as the vertexes, triangles all adopt the highly symmetric D_{3h} structure and tetragons are all in D_{2d} symmetry. In pentagons, only **5-Cl** adopts the highly symmetric D_{5h} structure, whereas **5-F** and **5-Br** are both in lower C_2 symmetry. In hexagons, **6-F** adopts the relatively symmetric D_{3d} structure, while **6-Cl** and **6-Br** both adopt a little lower S_6 structure. Note that the hexagonal frameworks of **6-Cl** and **6-Br** are obviously distorted from the planar arrangement (see their bottom view in Fig. 3), similar to the situations found for **7-NH_2** and **8-PH_2**. The HOMO-LUMO gaps for ***n*-E** (E = F, Cl, Br) polygons range from 6.76 to 7.68 eV at the B3LYP/def2-TZVPP level, suggesting the persistence of good electronic structures. The Be-Be distances in these polygons range from 1.748 to 1.759 Å, a little shorter than ***n*-E** (E = NH_2, PH_2, and OH) polygons, possibly due to the smaller repulsion effect since there have no H atom on halogen atoms.

Following the suggestion of a reviewer, we also selected the hexagons **6-E** (E = F, Cl, Br, OH, and SH) as the representatives for the calculations at the M06-2X-D3/def2-TZVPP level to calibrate the B3LYP functional. Only the **6-SH** adopt the different structure (C_1) from that obtained at the B3LYP level (D_{3d}). Such a distortion can be attribute to the flexibility of large molecules as witnessed in the B3LYP-optimized heptagons and octagons. So B3LYP and M06-2X-D3 results are essentially similar and the former should be reliable.

We also tried to substitute the H atoms on NH_2, PH_2, OH, and SH moieties with methyl groups to examine whether the

View Article Online
DOI: 10.1039/C9DT03322J

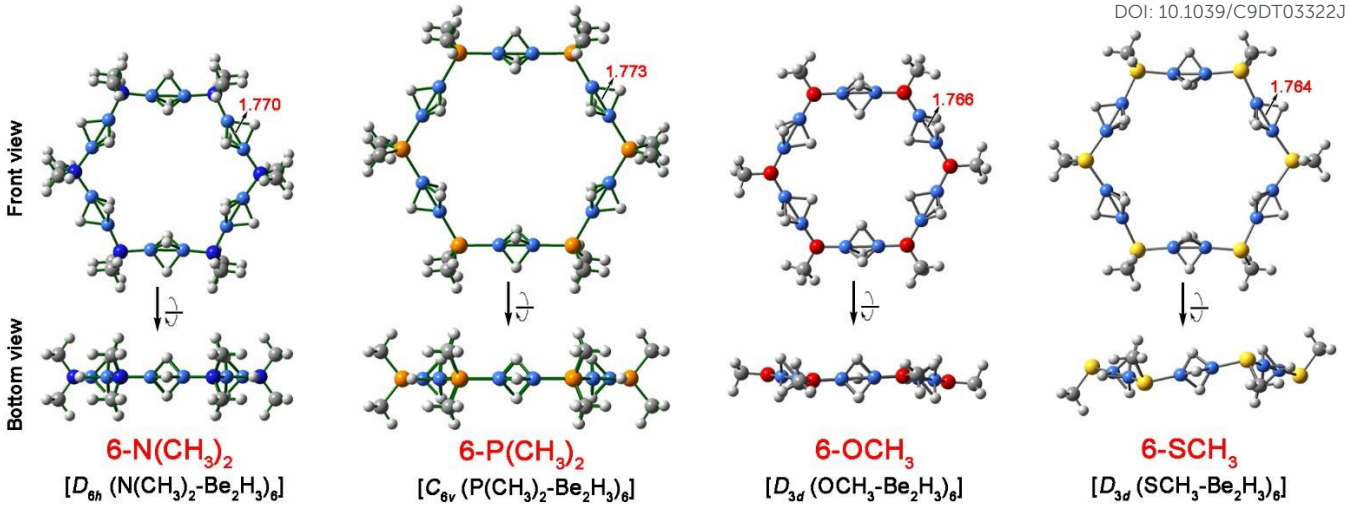

Fig. 4. B3LYP/def2-TZVPP-optimized structures of hexagons with $N(CH_3)_2$, $N(CH_3)_2$, OCH_3, and SCH_3 moieties as the vertexes.

structures and stabilities will be significantly influenced by the substitution. The triangles to hexagons for ***n*-N(CH$_3$)$_2$**, ***n*-P(CH$_3$)$_2$**, ***n*-OCH$_3$**, and ***n*-SCH$_3$** were constructed for demonstration. At the B3LYP/def2-TZVPP level, ***n*-N(CH$_3$)$_2$** (n = 3–6) and ***n*-P(CH$_3$)$_2$** (n = 3–5) adopt the highly symmetric D_{nh} structures, while the **6-P(CH$_3$)$_2$** is a little distorted to lower C_{6v} structure. In ***n*-OCH$_3$** and ***n*-SCH$_3$** (n = 3–6) polygons, only **6-OCH$_3$** and **6-SCH$_3$** adopt the same symmetry (D_{3d}, see Fig. 4) to their patent molecules **6-OH** and **6-SH**. The ***n*-OCH$_3$** (n = 3–5) are in C_{3v}, C_{2h}, and C_{5v} symmetries, respectively, while the ***n*-SCH$_3$** (n = 3–5) are in C_{3v}, D_{2d}, and C_{5v} symmetries, respectively. The Be-Be distances become a little longer after the methyl-substitution, possibly because of the larger repulsion effect of methyl groups than that of H atoms. Interestingly, as shown in Table 1, the methyl-substitution leads to the widened HOMO-LUMO gaps (by 0.35–0.55 eV) in ***n*-N(CH$_3$)$_2$** and ***n*-OCH$_3$** (n = 3–6) polygons, but the narrowed HOMO-LUMO gaps (by 0.25–0.61 eV) in ***n*-P(CH$_3$)$_2$** and ***n*-SCH$_3$** (n = 3–6) polygons

2. Electronic structures

To better understand the chemical bonding in these nano-polygons, we had performed the adaptive natural density partitioning (AdNDP)[9] analysis. As an extension to conventional natural bond orbital (NBO)[10] analysis, the AdNDP analysis can describe the bonding in a molecule using n-center two-electron bonds, where n ranges from one to the total number of atoms in the molecule. In general, the electron densities were partitioned with n values as small as possible, so AdNDP analysis

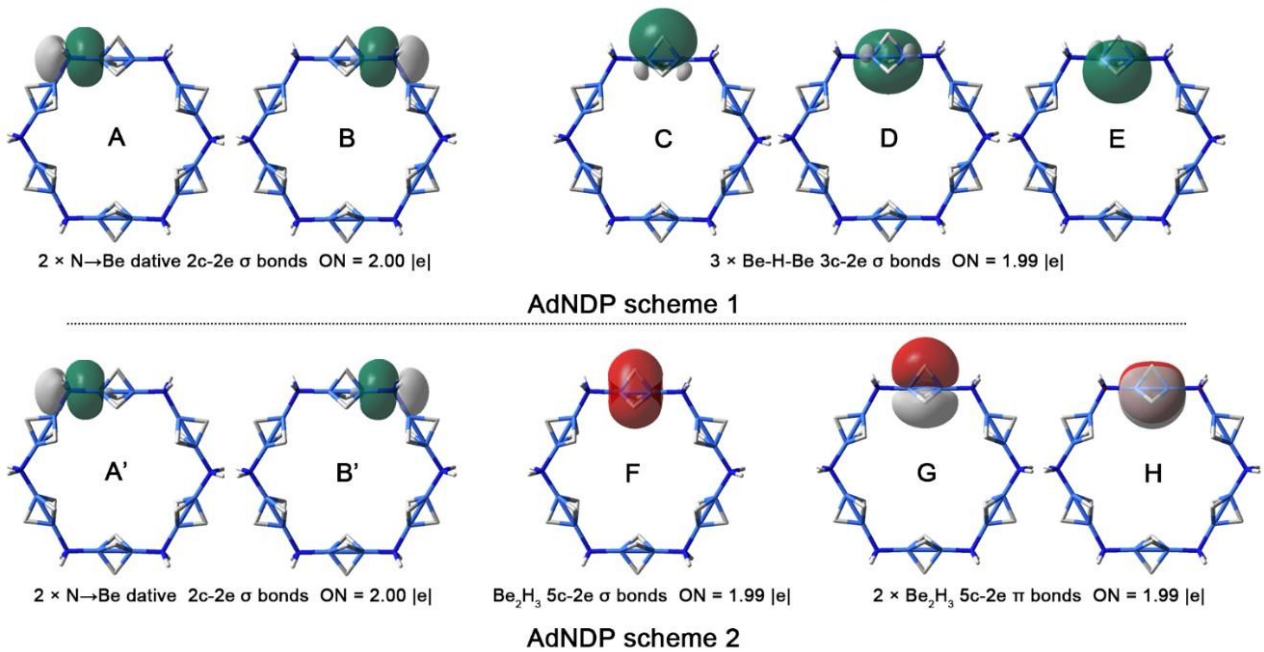

Fig. 5. Two schemes for AdNDP view of chemical bonding concerning one of Be_2H_3 moieties in **6-NH$_2$**. Two phases in scheme 1 and the 2c-2e bonds in scheme 2 are shown in green and white, respectively, while those for 5c-2e bonds in scheme 2 are shown in red and white, respectively.

View Article Online
DOI: 10.1039/C9DT03231

provides a very clear way to understand the chemical bonding. Alternatively, the AdNDP orbitals can be generated to adapt the requirement of bonding analysis. In this work, we employ the orbitals concerning one of Be_2H_3 moieties in **6-NH$_2$** as an example to describe the bonding in these nano-polygons. The AdNDP scheme 1 with *n* values as small as possible are shown in the first row of Fig. 5. As this scheme shows, there are two N→Be dative two-center two-electron (2c-2e) σ bonds with the occupation number (ON) of 2.00 |e| (see orbitals **A** and **B**). Noticeably, with the support of **A** and **B**, three Be-H-Be 3c-2e σ bonds with ON of 1.99 |e| are formed between two Be atoms (**C**–**E**). Although they are formed with the aid to three bridging H atoms, they are bonding orbitals for Be-Be interactions, which can significantly shorten the Be-Be distance. Such a bonding situation can be better understood using the alternative AdNDP scheme 2 (see the second row in Fig. 5). In such a scheme, two N→Be dative bonds in scheme 2 are retained (orbitals **A'** and **B'**), while three Be-H-Be 3c-2e σ bonds are repartitioned into three 5c-2e bonds (**F**–**H**) with ONs all at 1.99 |e|. It is remarkable that orbital **F** has no nodal surface passing Be-Be axis, which can be seen as a non-classical counterpart of classical 2c-2e σ bond; while orbitals **G** and **H** are orthogonal and both have a nodal surface passing the Be-Be axis, which can be regarded as the non-classical counterparts of two classical 2c-2e π bonds. In total, orbitals **F**–**H** can be seen as the non-classical counterpart of a classical triple bond and should play the similar role for shortening the Be-Be distance. The AdNDP results for other representative species are very similar to those of **6-NH$_2$**, thus they are given in the Fig. S4 to Fig. S10 in †ESI. The AdNDP view of chemical bonding in these polygonal species are very similar to their parent molecules, NH_3-Be_2H_3-NH_3^+ and PH_3-Be_2H_3-PH_3^+.[5g] Therefore, it is not curious that the polygons inherit the well-defined electronic structures from them.

We also performed the traditional NBO analyses to give more insight into the chemical bonding in these nano-polygons. The ionic bonding can be accessed the natural charge distribution, which are shown in the Table S1. The natural charges for ***n*-XH$_2$** (*n* = 3–6, X = N, P) are also marked on the molecules in Fig. 2. As the figure shows, all ***n*-XH$_2$** polygons adopt the alternate "– + –" charge distribution manner, *i.e.* the H (bridging), Be, and X carry the negative, positive, and negative charges, respectively, which is a type of favorable electrostatic interaction. Other polygons except for **6-P(CH$_3$)$_2$** have similar charge distribution manner, while for **6-P(CH$_3$)$_2$**, P atom possess the positive charges due to the methyl substitution (C is more electronegative than P). The charge distribution suggest that the majority of polygons benefit from the favourable ionic bonding.

The covalent bonding was evaluated by the Wiberg bond indices (WBIs). As shown in Table S1, the total WBI values for bridging H (H_{BR}) range from 0.95 to 1.00, consistent with the monovalent feature of H atom. The WBI_{Be} values in the polygons are all obviously higher than 2.00 (2.24 to 2.88). Such result seems to be contradicted with two valence electrons of Be. However, given that beryllium shows the typical electron deficient properties, it is not curious that the WBI_{Be} values are higher than 2.00 when beryllium is involved in the multicenter bonding. The $WBI_{X\text{-}Be}$ values range from 0.38 to 0.90, obviously smaller than 1.00, suggesting the relatively weak covalent X-Be and corroborating the relatively strong X-Be ionic bonding. The $WBI_{Be\text{-}H}$ values, ranging from 0.36 to 0.51, are consistent with the formation of Be-H-Be 3c-2e bonds, while the $WBI_{Be\text{-}Be}$ values of 0.42–0.53 revealed the significant direct Be-Be bonding.

3. Stability consideration

The polygons are too big for our computational resources to explore the potential energy surfaces and run the dynamic simulations at DFT level. In this work, the stability of nano-polygons was considered in two aspects: (1) the tendency of electron losing, gaining, and excitation; (2) the formation energies relative to basic building blocks (E^- and $Be_2H_3^+$).

As shown in Table 1, the nano-polygons possess the relatively large HOMO-LUMO gaps (6.20 to 7.68 eV). Such values suggest that it should be very difficult to excite the electrons from the occupied orbitals to the vacuum orbitals. To evaluate the electron losing and gain properties, we had calculated the vertical detachment energies (VDEs) and vertical electron affinities (VEAs) using outer valence Green's function (OVGF)[11] at the OVGF/def2-TZVPP level. As shown in Table 1, the VDEs of 8.96–11.29 eV indicate that it would be very hard for the polygons to lose an electron. Simultaneously, the VEAs of –1.05 to –1.21 eV in ***n*-NH$_2$** and ***n*-PH$_2$** (*n* = 3–6) indicate that they have low tendency to obtain the electron, while the VEAs of 0.86–1.78 eV in other ***n*-E** (*n* = 3–6) polygons indicate that they have no tendency to gain the electron. Being difficult to excite and detach the electron in them and having low or no tendency to obtain the electron, the polygons designed in this work should be very stable nano-molecules with regard to the electronic structure point of view.

The thermodynamic stability of the polygons was evaluated using the formation energies (FEs) relative to basic building blocks (E^- and $Be_2H_3^+$). The FEs are calculated using following equations (Eq.s):

$$nE^- + nBe_2H_3^+ \rightarrow (E\text{-}Be_2H_3)_n + FE_{total} \quad \text{Eq. 1}$$

$$FE_{X\text{-}E} = FE_{total} / 2n \quad \text{Eq. 2}$$

The FE_{total} and $FE_{X\text{-}Be}$ in the equations denote the total FEs and the average FEs for the formation of a X-Be bond. The $FE_{X\text{-}E}$ values are shown in Table 1. The $FE_{X\text{-}Be}$ values in polygons designed in this work range from 105.2 to 153.2 kcal/mol, being unexpectedly high and suggesting that the bonding between X and Be atoms should very strong and corresponding polygons should be very stable thermodynamically. The polygons with E atoms in the second row in the Periodic Table (*i.e.* N, O, and F) have the relatively high $FE_{X\text{-}Be}$ values of –135.9 to –153.2 kcal/mol. Those with E atoms in the third and fourth rows (*i.e.* P, S, Cl, and Br) have the relatively low $FE_{X\text{-}Be}$ values of –105.2 and –127.6 kcal/mol. Such differences can be explained by the hard-soft (Lewis) acid-base (HSAB) theory, *i.e.* the Be atom in the polygons is formally the dicationic Be^{2+}, which is a hard acid and thus exhibits the higher affinity to the hard bases like NH_2^-, $N(CH_3)_2^-$, OH^-/OCH_3^-, and F^- than to the intermediate or soft bases of $PH_2^-/P(CH_3)_2^-$, SH^-/SCH_3^-, Cl^-, and Br^-.

Conclusions

We had computationally designed a series of neutral nano-polygons ***n*-E** (*n* = 3–8, E = NH_2, PH_2, OH, SH, F, Cl, Br, $N(CH_3)_2$, $P(CH_3)_2$, OCH_3, and SCH_3) with ultrashort Be-Be distances. These nano-polygons have good stability with regard to electronic structures and thermochemistry, which can be demonstrated by the large HOMO-LUMO gaps, high VDEs, low or positive VEAs, and the unexpectedly high formation energies relative to building blocks. These nano-polygons should be the proper synthetic targets for experimental realization of ultrashort metal-metal distances between main group metals, which benefit the possible exploration of their application. We invite the chemical synthesis of these interesting and promising nano-molecules to push the main group metal-metal bonding chemistry forward.

Computational methods

The molecules designed in this work were optimized and harmonic vibrational frequencies were analysed at the B3LYP/def2-TZVPP level. The species **1**, **1'**, **2**, **2'**, ***n*-XH_2** (*n* = 3–5, X = N, P) were selected as the representatives for the re-optimization using both M06-2X-D3[8] functional and *ab initio* method MP2 to calibrate the B3LYP functional. Except for **4-NH_2** and **4-PH_2**, which adopted the slightly different geometries concerning the rotational freedom of bridging hydrogen atoms after calibrating calculations, other species adopted similar optimized geometries and vibrational frequencies to those obtained using B3LYP functional. Therefore, it should be safe to use B3LYP functional to study the polygonal species reported in this work. The adaptive natural density partitioning (AdNDP)[9] and natural bond orbital (NBO)[10] analyses were carried out at the B3LYP/6-31G and B3LYP/def2-TZVPP level, respectively, to better understand the chemical bonding in these nano-polygons. The vertical detachment energy (VDE) and vertical electron affinity (VEA) were calculated using outer valence Green's function (OVGF)[11] procedure at the OVGF/def2-TZVPP level. The formation energies for nano-polygons (relative to XH_2^- and $Be_2H_3^+$ building blocks) were calculated at the B3LYP/def2-TZVPP level with the consideration of Gibbs free energy corrections at 298 K. The AdNDP analyses were performed using AdNDP program,[12] the NBO analyses were carried out using NBO program embedded in GAUSSIAN 09 package,[13] while all other calculations were performed using GAUSSIAN 16 package.[14]

Conflicts of interest

There are no conflicts to declare.

Acknowledgements

The authors acknowledge support for this work from NSFC (Grant Nos. 21720102006, 21273140 and 21471092), the One Hundred-Talent Program of Shanxi Province, the OIT Program, Shanxi "1331 Project" Engineering Research Center (PT201807), the Shanxi 1331KIRT, and the High-Performance Computing Center of Shanxi University.

Notes and references

1 (a) F. R. Wagner, A. Noor and R. Kempe, *Nat. Chem.*, 2009, **1**, 529-536; (b) A. Noor and R. Kempe, *Inorg. Chim. Acta*, 2015, **424**, 75-82; (c) R. H. D. Lyngdoh, H. F. Schaefer and R. B. King, *Chem. Rev.*, 2018, **118**, 11626-11706.

2 (a) T. Nguyen, A. D. Sutton, M. Brynda, J. C. Fettinger, G. J. Long and P. P. Power, *Science*, 2005, **310**, 844-847; (b) G. Frenking, *Science*, 2005, **310**, 796-797; (c) K. A. Kreisel, G. P. A. Yap, O. Dmitrenko, C. R. Landis and K. H. Theopold, *J. Am. Chem. Soc.*, 2007, **129**, 14162-14163; (d) C.-W. Hsu, J.-S. K. Yu, C.-H. Yen, G.-H. Lee, Y. Wang and Y.-C. Tsai, *Angew. Chem., Int. Ed.*, 2008, **47**, 9933-9936; (e) A. Noor, F. R. Wagner and R. Kempe, *Angew. Chem., Int. Ed.*, 2008, **47**, 7246-7249; (f) Y.-C. Tsai, C.-W. Hsu, J.-S. K. Yu, G.-H. Lee, Y. Wang and T.-S. Kuo, *Angew. Chem., Int. Ed.*, 2008, **47**, 7250-7253; (g) A. Noor, G. Glatz, R. Mueller, M. Kaupp, S. Demeshko and R. Kempe, *Z. Anorg. Allg. Chem.*, 2009, **635**, 1149-1152; (h) A. Noor and R. Kempe, *Chem. Rec.*, 2010, **10**, 413-416; (i) L.-C. Wu, C.-W. Hsu, Y.-C. Chuang, G.-H. Lee, Y.-C. Tsai and Y. Wang, *J. Phys. Chem. A*, 2011, **115**, 12602-12615; (j) Y.-L. Huang, D.-Y. Lu, H.-C. Yu, J.-S. K. Yu, C.-W. Hsu, T.-S. Kuo, G.-H. Lee, Y. Wang and Y.-C. Tsai, *Angew. Chem., Int. Ed.*, 2012, **51**, 7781-7785; (k) A. Noor, T. Bauer, T. K. Todorova, B. Weber, L. Gagliardi and R. Kempe, *Chem.-Eur. J.*, 2013, **19**, 9825-9832; (l) V. E. Bondybey and J. H. English, *Chem. Phys. Lett.*, 1983, **94**, 443-447; (m) B. O. Roos, A. C. Borin and L. Gagliardi, *Angew. Chem., Int. Ed.*, 2007, **46**, 1469-1472; (n) F. Weinhold and C. R. Landis, *Science*, 2007, **316**, 61-63; (o) T. Alonso-Lanza, J. W. Gonzalez, F. Aguilera-Granja and A. Ayuela, *J. Phys. Chem. C*, 2017, **121**, 25554-25560; (p) L. J. Clouston, R. B. Siedschlag, P. A. Rudd, N. Planas, S. Hu, A. D. Miller, L. Gagliardi and C. C. Lu, *J. Am. Chem. Soc.*, 2013, **135**, 13142-13148; (q) S. P. Ranajit Saha, G. Merino, and P. K. Chattara, *Angew. Chem. Int. Ed.*, 2019, **131**, 8460 –8465; (r) A. Velazquez, I. Fernández, G. Frenking and G. Merino, *Organometallics*, 2007, **26**, 4731-4736.

3 (a) A. Noor, G. Glatz, R. Muller, M. Kaupp, S. Demeshko and R. Kempe, *Nat. Chem.*, 2009, **1**, 322-325; (b) A. Noor, E. S. Tamne, S. Qayyum, T. Bauer and R. Kempe, *Chem.-Eur. J.*, 2011, **17**, 6900-6903; (c) C. Schwarzmaier, A. Noor, G. Glatz, M. Zabel, A. Y. Timoshkin, B. M. Cossairt, C. C. Cummins, R. Kempe and M. Scheer, *Angew. Chem., Int. Ed.*, 2011, **50**, 7283-7286; (d) J. Shen, G. P. A. Yap, J.-P. Werner and K. H. Theopold, *Chem. Commun.*, 2011, **47**, 12191-12193; (e) E. S. Tamne, A. Noor, S. Qayyum, T. Bauer and R. Kempe, *Inorg. Chem.*, 2013, **52**, 329-336; (f) A. Noor, S. Qayyum, T. Bauer, S. Schwarz, B. Weber and R. Kempe, *Chem. Commun.*, 2014, **50**, 13127-13130; (g) J. Shen, G. P. A. Yap and K. H. Theopold, *Chem. Commun.*, 2014, **50**, 2579-2581; (h) J. M. Shen, G. P. A. Yap and K. H. Theopold, *Chem. Commun.*, 2014, **50**, 2579-2581; (i) A. K. Nair, N. V. S. Harisomayajula and Y. C. Tsai, *Inorg. Chim. Acta*, 2015, **424**, 51-62 and the references therein; (j) E. S. Tamne, A. Noor, T. Bauer and R. Kempe, *J. Organomet. Chem.*, 2016, **821**, 150-153.

4 M. Kaupp and P. v. R. Schleyer, *J. Am. Chem. Soc.*, 1993, **115**, 1061-1073.

5 (a) Z.-H. Cui, W.-S. Yang, L. Zhao, Y.-H. Ding and G. Frenking, *Angew. Chem., Int. Ed.*, 2016, **55**, 7841-7846; (b) C. Yuan, X.-F. Zhao, Y.-B. Wu and X. Wang, *Angew. Chem., Int. Ed.*, 2016, **55**, 15651-15655; (c) Q. Zhang, W.-L. Li, L. Zhao, M. Chen, M. Zhou, J. Li and G. Frenking, *Chem.-Eur. J.*, 2017, **23**, 2035-2039; (d) W.-Y. Tong, T.-T. Zhao, and Y.-B. Wu, *J. Shanxi Univ., Nat. Sci. Ed.*, 2020, **43**, DOI: 10.13451/j.cnki.shanxi.univ(nat.sci.). 2019.05.10.002; (e) T.-T. Zhao, X.-F. Zhao, J.-H. Bian, W.-Y.

View Article Online
DOI: 10.1039/C9DT03322J

Tong, B. Jin, X. Wang, C. Yuan, and Y.-B. Wu, *Dalton Trans.*, 2019, **48**, 6581-6587. (f) Z. Z. Qin, Q. Wang, C. X. Yuan, Y. T. Yang, X. F. Zhao, D. B. Li, P. Liu and Y. B. Wu, *Dalton Trans.*, 2018, **47**, 4707-4713; (g) X.-F. Zhao, C. Yuan, S.-D. Li, Y.-B. Wu and X. Wang, *Dalton Trans.*, 2018, **47**, 14462-14467; (h) R. Saha, S. Pan, G. Merino, and P. K. Chattara, *Angew. Chem.*, 2019, **131**, 8460-8465; (i) A. Velazquez, I. Fernández, G. Frenking and G. Merino, *Organometallics*, 2007, **26**, 4731-4736.

6 Z. Z. Li, A. Y. Li and L. F. Ji, *J. Phys. Chem. A*, 2015, **119**, 8400-8413.

7 The located lowest energy isomers and relative energies for these species are given in Fig. S1 in †ESI.

8 (a) Y. Zhao and D. G. Truhlar, *Theor. Chem. Acc.* 2008, **120**, 215-241. (b) S. Grimme, S. Ehrlich, and L. Goerigk, *J. Comp. Chem.* 2011, **32**, 1456-1465.

9 D. Y. Zubarev and A. I. Boldyrev, *J. Org. Chem.*, 2008, **73**, 9251-9258.

10 A. E. Reed, L. A. Curtiss and F. Weinhold, *Chem. Rev.*, 1988, **88**, 899-926.

11 J. V. Ortiz, V. G. Zakrzewski and O. Dolgounircheva, *Conceptual Perspectives in Quantum Chemistry*, Kluwer Academic, 1997.

12 The AdNDP program was downloaded at http://ion.chem.usu.edu/~boldyrev/adndp.php.

13 M. J. Frisch *et al*., in *Gaussian 09 Revision D. 01*, Gaussian Inc. Wallingford, CT, 2013.

14 M. J. Frisch *et al*., in *Gaussian 16 Revision A. 03*, Gaussian Inc. Wallingford, CT, 2016.

View Article Online
DOI: 10.1039/C9DT03322J

TOC entry:

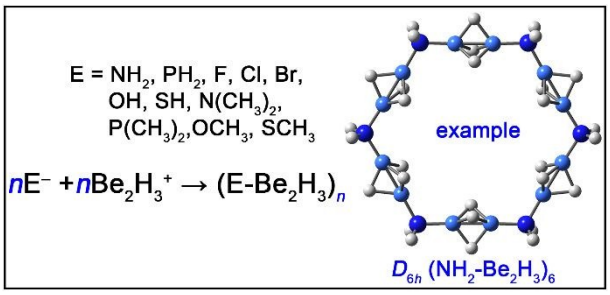

DFT calculations revealed that neutral polygons $(E\text{-}Be_2H_3)_n$ were the viable targets for realizing ultrashort metal-metal distances between main group metal.